Available online at www.sciencedirect.com
SCIENCE DIRECT®
Journal of Sound and Vibration 275 (2004) 177–191
JOURNAL OF SOUND AND VIBRATION
www.elsevier.com/locate/jsvi

Non-linear vibrations of a beam with cantilever-Hertzian contact boundary conditions

J.A. Turner*

Department of Engineering Mechanics, University of Nebraska-Lincoln, W317.4 Nebraska Hall, Lincoln, NE 68588-0526, USA

Received 24 July 2002; accepted 23 June 2003

Abstract

The non-linear vibrations of a linear beam with cantilever-Hertzian contact boundary conditions are investigated. The method of multiple scales is used to analyze this problem in which it is assumed that the beam remains in contact with the moving surface at all times. One primary result from this analysis is the amplitude–frequency relation for the various flexural modes. The amplitude–frequency curves exhibit softening behavior as expected. The amount of softening is shown to depend on the linear contact stiffness as well as the specific mode. In addition, the associated non-linear normal modes of this system are derived. The modes include a non-linear modification to the linear, harmonic component as well as a static offset term and second and third harmonic components.

1. Introduction

The dynamics of moving surfaces that are in contact with each other is important in a number of scientific and engineering applications. The vibrations of such contacts have been examined previously by a number of authors [1–3]. The focus in these studies was primarily on a single-degree-of-freedom (SDOF) system in Hertzian contact with a moving surface. Although Bryant [2] was interested in the vibrations of a beam in Hertzian contact, for modelling actuator dynamics, the beam was ultimately simplified to a SDOF system as well. The flexural vibrations of beams with non-linearities has been examined in a variety of other forms using many different methods. Non-linear vibrations of linearly elastic beams with non-linear boundary conditions

*Corresponding author. Tel.: +1-402-472-8856; fax: +1-402-472-8292.
E-mail address: jaturner@unl.edu (J.A. Turner).
URL: http://em-jaturner.unl.edu.

0022-460X/$ - see front matter © 2003 Elsevier Ltd. All rights reserved.
doi:10.1016/S0022-460X(03)00791-0

have been studied far less using techniques including the harmonic balance method [4], the method of Shaw and Pierre [5], and the method of multiple scales [6]. Non-linear normal modes have been observed in many other contexts as well [7].

More recently, the problem of a cantilevered beam in Hertzian contact with a moving surface has been applied to atomic force microscope (AFM) applications [8,9]. Dynamic AFM methods rely on the relative motion between the AFM tip and the specimen surface. These techniques are used to extract quantitative information about the surface stiffness with high resolution [9]. These techniques utilize the dynamic response of the AFM beam, specifically in terms of the flexural cantilever modes. A stiff cantilever with high contact force is typically used to confine the tip–surface forces to the Hertzian contact regime. In these studies, the amplitude of the surface motion is kept small such that the motion may be analyzed by linearizing the non-linear tip–surface interaction forces. Such linearization has proven very effective for a variety of materials. As the surface amplitude increases, the motion eventually becomes non-linear. If the motion is very large, the non-linear motion is chaotic [10]. Before chaotic motion occurs however, there is a range of non-linear motion that is stable. It is anticipated that a perturbation approach may be applicable to describe this motion. It is in this regime that the effects of this softening non-linearity have been observed experimentally in terms of the shifts of resonant frequencies as a function of amplitude [8]. The method of harmonic balance was recently used to examine a similar contact AFM vibration problem [11].

In this article, the non-linear vibrations of an elastic beam with cantilever-Hertzian contact boundary conditions are examined. It is assumed throughout that the beam remains in contact with the vibrating surface at all times. In addition, the vibrational amplitude in the beam is assumed to remain small such that the beam remains in the linear regime. Experimental evidence suggests that the beam loses contact before non-linear effects in the beam are important [8]. In the next section, the appropriate boundary value problem is described. The method of multiple scales is then used to analyze this problem. The primary results from this analysis include the amplitude–frequency relation for the various flexural modes as well as the non-linear normal modes. Finally, example results are presented. It is shown that the non-linear behavior, in terms of the non-linear frequency shift and the change in mode shape, are sensitive to the particular mode and to the linear contact stiffness. The dependence on the non-linear parameters of the problem is clearly defined. The theoretical results have the same qualitative features as experimental AFM results. A similar type of analysis was also recently used to examine the non-linear vibrations of the first flexural mode when the AFM tip is under the influence of a Lennard-Jones potential [12].

2. Problem description

A uniform, homogeneous beam of constant cross-section is cantilevered at one end as depicted in Fig. 1. At the end opposite of the cantilever ($x = L$), a massless tip with small radius is attached. The tip is in contact with a surface as shown. The boundary value problem for this system has a governing equation given by

$$EIq''''(x,t) + \rho A\ddot{q}(x,t) = 0 \tag{1}$$

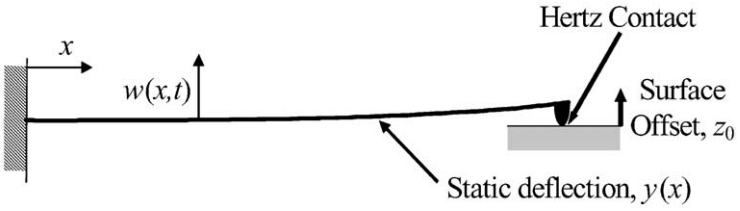

Fig. 1. Schematic of the problem. The linearly elastic beam is in contact with a surface. Initial contact is made when the surface offset, z_0, is zero. This static offset causes a static beam deflection, $y(x)$. The dynamic motion, $w(x,t)$, is defined relative to $y(x)$. The contact forces between the tip and sample are assumed Hertzian with no attractive forces.

with boundary conditions

$$q(x,t) = 0 \quad \text{at } x = 0, \quad q'(x,t) = 0 \quad \text{at } x = 0, \quad q''(x,t) = 0 \quad \text{at } x = L, \tag{2–4}$$

$$EIq'''(x,t) - 3\frac{EI}{L^3}y(L) + K_0[z_0 - y(L) - q(x,t)]^{3/2} = 0 \quad \text{at } x = L. \tag{5}$$

In Eqs. (1)–(5), $q(x,t)$ defines the cantilever position relative to its initial static deflection $y(x)$. Also, the primes indicate spatial derivatives, while the overdots indicate time derivatives. The beam is defined by the modulus E, the area moment of the cantilever I, the volume density ρ, and the cross-sectional area A. Here, EI and ρA are assumed uniform over the length of the beam. The boundary conditions given by Eqs. (2)–(4) correspond to conditions of zero displacement and zero slope at $x = 0$, and zero moment at $x = L$.

The boundary condition given by Eq. (5) is the force balance between the shear force in the beam and the interaction force associated with the tip and the surface. Here, this interaction force is assumed to be the Hertzian contact condition of a sphere in contact with a plane [13,14]. It is through this contact that the non-linear behavior of the beam manifests itself. Therefore, the specific properties of the contact interaction, such as adhesion, friction, and attractive forces, will have a profound effect on the non-linear behavior of the beam. Regardless of the form of the non-linear contact, the perturbation analysis formulated here will be similar. The use of Hertzian theory in this article provides the first step towards the analysis of more complex contact forces. In Eq. (5), the Hertz coefficient, $K_0 = \frac{4}{3}E^*\sqrt{R}$, is defined in terms of the reduced elastic modulus, E^*, and the tip radius, R. The reduced modulus is defined by the material properties (elastic modulus, E, and Poisson's ratio, v) of the surface and tip. It is defined by

$$\frac{1}{E^*} = \frac{1 - v_t^2}{E_t} + \frac{1 - v_s^2}{E_s}, \tag{6}$$

where the subscripts t and s denote the tip and surface, respectively.

The function $y(x)$ in Eq. (5) defines the static deflection of the cantilever due to the surface offset. A static offset results from changes in the relative position between the beam and the surface. The end deflection, $y(L)$, will be slightly less than the surface offset, z_0. The difference between the two is the result of deformation. The end deflection is defined by consideration of the

static problem. The initial deflection of the cantilever is written in terms of the end deflection as

$$y(x) = \frac{1}{2} y(L) \left(\frac{x}{L}\right)^2 \left(3 - \frac{x}{L}\right). \tag{7}$$

The end deflection is governed by

$$-3\frac{EI}{L^3} y(L) + K_0 (z_0 - y(L))^{3/2} = 0, \tag{8}$$

which defines $y(L)$ in terms of the surface offset, z_0. Without loss of generality, it is assumed that z_0 is zero when the tip first comes in contact with the surface. This assumption also implies that the cantilever is horizontal when it first makes contact with the surface. In Eqs. (5) and (8), the quantity $\Delta = z_0 - y(L)$ may be identified as the static Hertz deformation. Note that no attractive forces are assumed present.

The non-linear analysis which follows requires a more amenable form for the non-linear contact. The contact boundary condition (5) is first rewritten as

$$EIw'''(x,t) - 3\frac{EI}{L^3}(z_0/\Delta - 1) + K_0 \Delta^{1/2}[1 - w(x,t)]^{3/2} = 0 \quad \text{at } x = L, \tag{9}$$

where $w = q/\Delta$ defines the beam deflection relative to the static Hertz deformation. Note that the beam remains in contact with the surface as long as $w(L,t) \leqslant 1$. Finally, the term in Eq. (9) with the $3/2$ exponent is expanded in a Taylor series expansion about the equilibrium position, $w(L,t) = 0$. The result is

$$EIw''' = \kappa w - \kappa_1 w^2 - \kappa_2 w^3, \tag{10}$$

where the linear and non-linear spring constants are given by

$$\kappa = \tfrac{3}{2} K_0 \Delta^{1/2}, \quad \kappa_1 = \tfrac{3}{8} K_0 \Delta^{1/2}, \quad \kappa_2 = \tfrac{1}{16} K_0 \Delta^{1/2}. \tag{11}$$

The error in this expansion is less than 1% over the range in which the contact is not lost. A similar type of expansion has been successfully used to model Hertzian contact vibrations in single-degree of freedom systems [2,3].

3. Method of multiple scales

The non-linear vibration problem described in Section 2 is now solved using the method of multiple scales. The problem is first recast in dimensionless form. The governing equation is thus given by

$$\ddot{w} + w'''' = 0 \tag{12}$$

with boundary conditions

$$w = w' = 0 \quad \text{at } x = 0, \qquad w'' = 0 \quad \text{at } x = 1, \tag{13}$$

$$w''' - \beta w - \varepsilon^2 c\dot{w} + \varepsilon\beta_1 w^2 + \varepsilon^2 \beta_2 w^3 = \varepsilon^2 F \cos \Omega t \quad \text{at } x = 1, \tag{14}$$

where ε is a dimensionless parameter introduced to order the different scales of the problem. A viscous damping term (as observed experimentally) and a forcing term (typical of dynamic AFM experiments) have been added to the final boundary condition. A uniformly valid approximation

requires the damping, forcing, and the cubic non-linearity to occur at the same level of perturbation, in this case at ε^2 [15]. In Eqs. (12)–(14), the position along the beam is measured in units of L and time is measured in units of $\sqrt{(\rho AL)/(EI/L^3)}$. The dimensionless linear and non-linear spring constants are defined by

$$\beta = \frac{3}{2}\frac{K_0 \Delta^{1/2}}{EI/L^3}, \quad \beta_1 = \frac{\beta}{4}, \quad \beta_2 = \frac{\beta}{24}. \tag{15}$$

Thus, β defines the stiffness of the contact relative to the stiffness of the beam. The contact stiffnesses are determined by Δ which is related to the static offset through Eq. (8).

The method of multiple scales is applied to this non-linear boundary value problem [6]. We look for solutions of the form

$$w(x; T_0, T_1, T_2) = w_0(x; T_0, T_1, T_2) + \varepsilon w_1(x; T_0, T_1, T_2) + \cdots \tag{16}$$

where T_0, T_1, and T_2 are the different time scales of the problem, $T_n = \varepsilon^n t$. The expansion is substituted into Eqs. (12)–(14) and like orders of ε are collected. This procedure defines the ε^0 problem as

$$w_0'''' + D_0^2 w_0 = 0, \tag{17}$$

$$w_0 = w_0' = 0 \quad \text{at } x = 0, \qquad w_0'' = 0 \quad \text{at } x = 1, \tag{18}$$

$$w_0''' = \beta w_0 \quad \text{at } x = 1. \tag{19}$$

The ε^1 problem is given by

$$w_1'''' + D_0^2 w_1 = -2D_0 D_1 w_0, \tag{20}$$

$$w_1 = w_1' = 0 \quad \text{at } x = 0, \qquad w_1'' = 0 \quad \text{at } x = 1, \tag{21}$$

$$w_1''' = \beta w_1 - \beta_1 w_0^2 \quad \text{at } x = 1 \tag{22}$$

and for ε^2,

$$w_2'''' + D_0^2 w_2 = -2D_0 D_1 w_1 - (D_1^2 + 2D_0 D_2) w_0, \tag{23}$$

$$w_2 = w_2' = 0 \quad \text{at } x = 0, \quad w_2'' = 0 \quad \text{at } x = 1, \tag{24}$$

$$w_2''' = \beta w_2 + cD_0 w_0 - \beta_1 w_0 w_1 - \beta_2 w_0^3 - F\cos \Omega t \quad \text{at } x = 1. \tag{25}$$

Each of these problems is now solved.

3.1. Order ε^0 problem

The ε^0 problem has solution

$$w_0(x; T_0, T_1) = A_m(T_1, T_2) \mathrm{e}^{\mathrm{i}\omega_m T_0} W(x) + \mathrm{cc} \tag{26}$$

for the mth mode where cc denotes the complex conjugate of the previous expression. The modal subscripts on A_m and ω_m are implicit throughout the remainder of the article. The linear mode

shape $W(x)$ is given by

$$W(x) = W_0(\sin\gamma x - \sinh\gamma x - H_0(\cos\gamma x - \cosh\gamma x)), \tag{27}$$

where

$$W_0 = \frac{\cos\gamma + \cosh\gamma}{2(\sin\gamma\cosh\gamma - \sinh\gamma\cos\gamma)}, \quad H_0 = \frac{\sin\gamma + \sinh\gamma}{\cos\gamma + \cosh\gamma}. \tag{28}$$

The normalization factor W_0 is included to ensure that the displacement of the cantilever end $W(1)$ does not lose contact, such that $W(1) = 1$.

The values of the dimensionless wave numbers γ are determined from the characteristic equation of the linear problem

$$\gamma^3(\cosh\gamma\cos\gamma + 1) - \beta(\sinh\gamma\cos\gamma - \sin\gamma\cosh\gamma) = 0. \tag{29}$$

The wave numbers are related to the natural frequencies through the dispersion relation $\omega^2 = \gamma^4$.

3.2. Order ε^1 problem

The solution for w_0 is necessary for the order ε^1 problem. The problem for w_1 is given by

$$w_1'''' + D_0^2 w_1 = -2i\omega D_1 A e^{i\omega T_0} W(x) + cc, \tag{30}$$

$$w_1 = w_1' = 0 \quad \text{at } x = 0, \qquad w_1'' = 0 \quad \text{at } x = 1 \tag{31}$$

and the contact boundary condition is given by

$$w_1''' = \beta w_1 - \beta_1[A^2 e^{2i\omega_m T_0} + 2A\bar{A} + \bar{A}^2 e^{-2i\omega_m T_0}] \quad \text{at } x = 1. \tag{32}$$

First we seek solutions of the form

$$w_1(x; T_0, T_1, T_2) = g_1(x; T_1, T_2)e^{i\omega T_0}. \tag{33}$$

The problem for g_1 is then

$$g_1'''' - \omega^2 g_1 = -2i\omega D_1 A W(x) \tag{34}$$

with boundary conditions

$$g_1 = g_1' = 0 \quad \text{at } x = 0, \qquad g_1'' = 0 \quad \text{at } x = 1, \tag{35}$$

$$g_1'' = \beta g_1 \quad \text{at } x = 1. \tag{36}$$

Because the homogeneous equations for g_1 have a non-trivial solution, the non-homogeneous equations for g_1 have a solution only if a solvability condition is satisfied. By virtue of the characteristic equation defining γ, Eq. (29), the solvability condition implies that $D_1 A = 0$, or $A = A(T_2)$.

The two other parts of the w_1 solution are also found. One solution is of the form

$$w_1 = g_2(x)e^{2i\omega T_0}. \tag{37}$$

Thus, the solution is

$$g_2(x) = \frac{\beta_1 A^2}{2} G(\chi_2, x), \tag{38}$$

where $\chi_2 = \sqrt{2\omega}$ and the function $G(\chi, x)$ is defined as

$$G(\chi, x) = -\frac{(\cos\chi + \cosh\chi)(\sinh\chi x - \sin\chi x) + (\cos\chi x - \cosh\chi x)(\sin\chi + \sinh\chi)}{\chi^3(1 + \cos\chi\cosh\chi) - \beta(\sinh\chi\cos\chi - \sin\chi\cosh\chi)}. \tag{39}$$

The final part of the w_1 solution is related to the static shift due to the non-linearity. Such a response is expected in systems with quadratic non-linearities [6]. We look for solutions of the form

$$w_1 = g_0(x). \tag{40}$$

Substitution into the boundary conditions gives

$$g_0(x) = -\frac{\beta_1 A\bar{A}}{2(3+\beta)}x^2(x-3). \tag{41}$$

The complete solution for w_1 is thus

$$w_1 = -\frac{\beta_1 A\bar{A}}{2(3+\beta)}x^2(x-3) + \frac{\beta_1 A^2}{2}G(\chi_2, x)\mathrm{e}^{2\mathrm{i}\omega T_0} + \mathrm{cc}, \tag{42}$$

where A is found from the ε^2 problem. As expected, the w_1 solution is proportional to β_1 and quadratic in amplitude.

3.3. Order ε^2 problem

The solutions obtained for w_0 and w_1 are necessary for the order ε^2 problem. The ε^2 problem is written in terms of these solutions

$$w_2'''' + D_0^2 w_2 = -2\mathrm{i}\omega A'\mathrm{e}^{\mathrm{i}\omega T_0}W(x), \tag{43}$$

where $A' = D_2 A$. The appropriate boundary conditions are

$$w_2 = w_2' = 0 \quad \text{at } x = 0, \qquad w_2'' = 0 \quad \text{at } x = 1, \tag{44}$$

$$w_2''' = \beta w_2 + c\mathrm{i}\omega A\mathrm{e}^{\mathrm{i}\omega T_0} + \left(\beta_1^2 G(\chi_2, 1) - \frac{2\beta_1^2}{3+\beta} - 3\beta_2\right)A\bar{A}^2\mathrm{e}^{\mathrm{i}\omega T_0} + (\beta_1^2 G(\chi_2, 1) - \beta_2)A^3\mathrm{e}^{3\mathrm{i}\omega T_0} + \mathrm{cc}.$$

Next, we seek solutions of the form

$$w_2(x; T_0, T_2) = h_1(x; T_2)\mathrm{e}^{\mathrm{i}\omega T_0}. \tag{45}$$

The homogeneous equations for h_1 have a non-trivial solution. Thus, the non-homogeneous equations for h_1 require a solvability condition. This condition is

$$P(\gamma)\mathrm{i}\omega A' = c\mathrm{i}\omega A + \beta_1^2\bar{A}A^2\left(G(\chi_2, 1) - \frac{2}{3+\beta}\right) - 3\beta_2\bar{A}A^2, \tag{46}$$

where

$$P(\gamma) = \frac{3\gamma^2(\cos\gamma + \cosh\gamma)(1 + \cos\gamma\cosh\gamma) - \gamma^3 \sin\gamma \sinh\gamma(\sin\gamma + \sinh\gamma)}{\gamma^3(\cos\gamma + \cosh\gamma)^2} + \beta\frac{\sin\gamma\sinh\gamma(\cos\gamma + \cosh\gamma) + (1 + \cos\gamma\cosh\gamma)(\cosh\gamma - \cos\gamma)}{\gamma^3(\cos\gamma + \cosh\gamma)^2}.$$

The dependence of Eq. (46) on the particular mode is implicit in the factors of $P(\gamma)$ and $G(\chi_2, 1)$.

The solution for the harmonic component of w_2 is then

$$h_1(x) = \left[c\mathrm{i}\omega A + \beta_1^2\bar{A}A^2\left(G(\chi_2, 1) - \frac{2}{3+\beta}\right) - 3\beta_2\bar{A}A^2\right]H(x), \tag{47}$$

where

$$H(x) = \frac{1}{2\gamma^3 P(\gamma)}\left[(\cos\gamma x - \cosh\gamma x)\left(\frac{2(1 + \cos\gamma\cosh\gamma)}{(\cos\gamma + \cosh\gamma)^2} - x\right) - x\frac{\sin\gamma + \sinh\gamma}{\cos\gamma + \cosh\gamma}(\sin\gamma x + \sinh\gamma x)\right].$$

The final part of the solution for w_2 is found in a similar manner to that for g_2 in the order ε^1 problem. The solution is thus

$$h_3(x) = -\frac{A^3}{2}(\beta_1^2 G(\chi_2, 1) - \beta_2)G(\chi_3, x), \tag{48}$$

with $G(\chi, x)$ defined in Eq. (39) and $\chi_3 = \sqrt{3\omega}$.

The complete non-linear mode that tends to the linear mode when β_1 and β_2 tend to zero is then

$$\begin{aligned} w(x; T_0, T_2) = {} & (W(x) + \mathrm{i}c\omega H(x))A\mathrm{e}^{\mathrm{i}\omega_m T_0} \\ & + \left(\beta_1^2 G(\chi_2, 1) - \frac{2\beta_1^2}{3+\beta} - 3\beta_2\right)\bar{A}A^2 H(x)\mathrm{e}^{\mathrm{i}\omega T_0} - \frac{\beta_1 A\bar{A}}{2(3+\beta)}x^2(x-3) \\ & + \frac{\beta_1 A^2}{2}G(\chi_2, x)\mathrm{e}^{2\mathrm{i}\omega T_0} - \left(\frac{A^3}{2}(\beta_1^2 G(\chi_2, 1) - \beta_2)G(\chi_3, x)\right)\mathrm{e}^{3\mathrm{i}\omega T_0} + \mathrm{cc}, \end{aligned}$$

where A is defined by Eq. (46).

To solve Eq. (46) we look for solutions of the form $A = \frac{1}{2}p\mathrm{e}^{\mathrm{i}q}$ where p and q are real functions of T_2. Substitution into Eq. (46) gives

$$P(\gamma)(\mathrm{i}\omega p' - \omega p q') = c\mathrm{i}\omega p + \frac{1}{4}\beta_1^2 p^3\left(G(\chi_2, 1) - \frac{2}{3+\beta}\right) - \frac{3}{4}\beta_2 p^3 - 2F\mathrm{e}^{\mathrm{i}\sigma T_2 - \mathrm{i}q}. \tag{49}$$

Next we define $\psi = \sigma T_2 - q$ such that $q' = \psi' - \sigma$. Separating Eq. (49) into real and imaginary parts gives

$$P(\gamma)(-\omega p\psi' + \omega p\sigma) = \frac{\beta_1^2 p^3}{4}\left(G(\chi_2, 1) - \frac{2}{3+\beta}\right) - \frac{3}{4}\beta_2 p^3 - 2F\cos\psi, \tag{50}$$

$$P(\gamma)\omega p' = c\omega p - 2F\sin\psi. \tag{51}$$

Steady state motion occurs when $\psi' = p' = 0$. Thus,

$$2F\cos\psi = \frac{\beta_1^2 p^3}{4}\left(G(\chi_2, 1) - \frac{2}{3+\beta}\right) - \frac{3}{4}\beta_2 p^3 - P(\gamma)\omega p\sigma, \tag{52}$$

$$2F\sin\psi = c\omega p. \tag{53}$$

Eqs. (52) and (53) are squared and added. The result is solved for σ giving

$$\sigma = \frac{[\beta_1^2(G(\chi_2,1) - 2/(3+\beta)) - 3\beta_2]}{4P(\gamma)\omega}p^2 \pm \frac{1}{P(\gamma)\omega}\sqrt{\frac{4F^2}{p^2} - \omega^2 c^2}. \tag{54}$$

The detuning parameter σ is related to p in Eq. (54). The phase shift ψ is then found from

$$\psi = \tan^{-1}\left(\frac{4c\omega}{\beta_1^2 p^2(G(\chi_2,1) - 2/(3+\beta)) - 3\beta_2 p^2 - 4P(\gamma)\omega\sigma}\right), \tag{55}$$

such that $A = \frac{1}{2}pe^{i\sigma T_2 - i\psi}$. The maximum value for p is

$$p_{max} = \frac{2F}{c\omega}, \tag{56}$$

which occurs when

$$\sigma = \left(\frac{F}{c\omega}\right)^2 \frac{\beta_1^2(G(\chi_2,1) - 2/(3+\beta)) - 3\beta_2}{P(\gamma)\omega}. \tag{57}$$

In terms of the parameters p and q, the non-linear normal mode reduces to (damping has been dropped from the mode as discussed by Nayfeh [6])

$$\begin{aligned} w(x;T_0,T_2) = {} & \left(W(x)p + \left(\beta_1^2 G(\chi_2,1) - \frac{2\beta_1^2}{3+\beta} - 3\beta_2\right)H(x)\frac{1}{4}p^3\right)\cos(\omega T_0 + q) \\ & - \frac{\beta_1 x^2(x-3)}{4(3+\beta)}p^2 + \frac{\beta_1}{4}G(\chi_2,x)\,p^2\cos(2\omega T_0 + 2q) \\ & - (\beta_1^2 G(\chi_2,1) - \beta_2)G(\chi_3,x)\frac{1}{8}p^3\cos(3\omega T_0 + 3q). \end{aligned} \tag{58}$$

The non-linear amplitude–frequency relation (54), and the non-linear normal mode (58), are the main results of this derivation. The dependence of the non-linear response on the different modes is included in the amplitude–frequency relation by the functions P and G.

The various components of the non-linear normal mode include a harmonic component and static offset as well as second and third harmonic components. The static shift due to the non-linearity is proportional to $\beta_1/(3+\beta)$ and quadratic in amplitude. The spatial dependence of the second and third harmonics are proportional to $G(\chi,x)$, for $\chi = \chi_2$ or $\chi = \chi_3$, respectively. The second harmonic is quadratic in amplitude and proportional to β_1. The third harmonic is cubic in amplitude and dependent on β_1, β_2, and $G(\chi_2,1)$. In the next section, example results are presented using Eqs. (54), (58), and (39).

4. Example results

The non-linear amplitude–frequency behavior for several modes using Eq. (54) is first presented. It should be noted that the dependence of σ on the forcing amplitude F is inverse to the dependence of σ on damping c. Plots for fixed c and increasing F are presented in Figs. 2

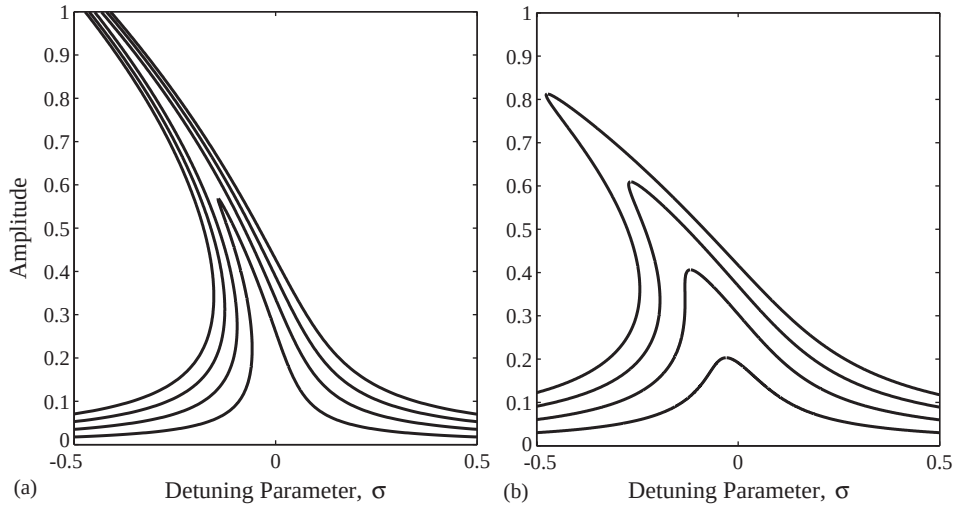

Fig. 2. Example results for the primary non-linear response for $\beta = 300$ and four values of F $(= 1, 2, 3, 4)$ with $c = 0.12$. The (a) first and (b) second modes are shown.

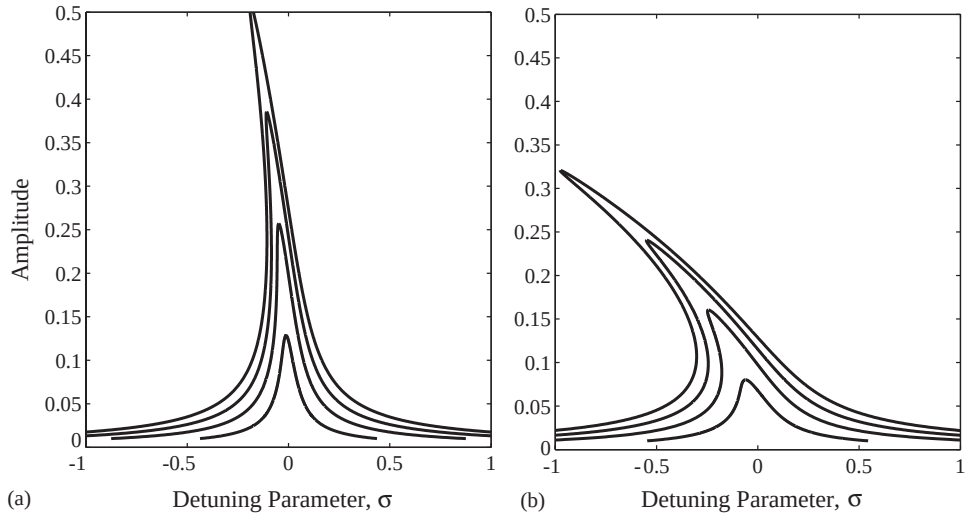

Fig. 3. Example results for the primary non-linear response for $\beta = 500$ and four values of F $(= 1, 2, 3, 4)$ with $c = 0.08$. The (a) third and (b) fourth modes are shown.

and 3. Similar behavior is observed for fixed F and decreasing c. Fig. 2 is a plot of amplitude versus σ for modes 1 and 2 for $\beta = 300$ and $c = 0.12$ for several values of F. The values of σ for both modes are of the same order over the range of amplitude shown, as large as -0.5. The response of mode 1 to the higher amplitudes ($F = 3, 4$, and 6) leads to a response that is larger than 1. In terms of the quantities defined here, these values would lead to a loss of contact. Mode 2, however, does not have a response larger than 1 for any of the values of forcing used. Similar results for modes 3 and 4 for $\beta = 1800$ and $c = 0.08$ are shown in Fig. 3.

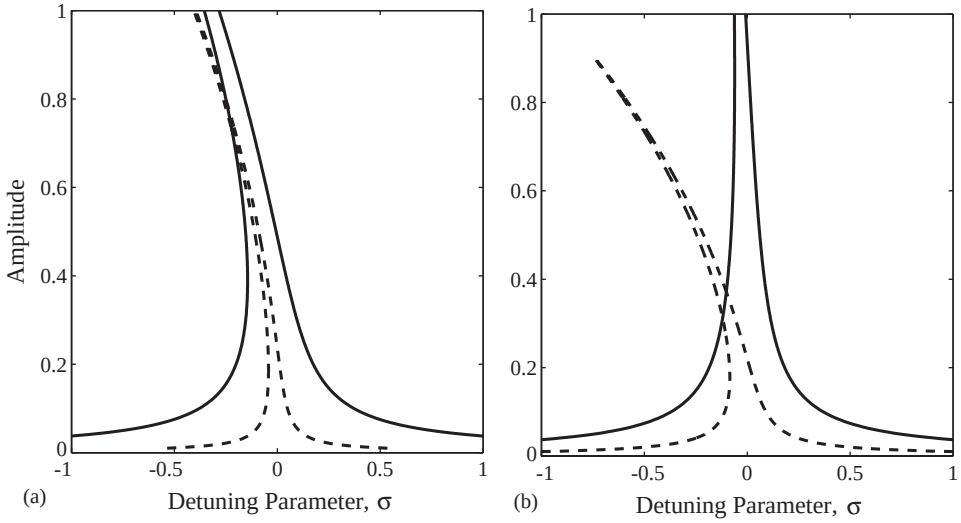

Fig. 4. Non-linear frequency shift of the (a) first and (b) second modes for two values of linear stiffness β (solid: $\beta = 50$; dashed: $\beta = 500$) with $c = 0.025$.

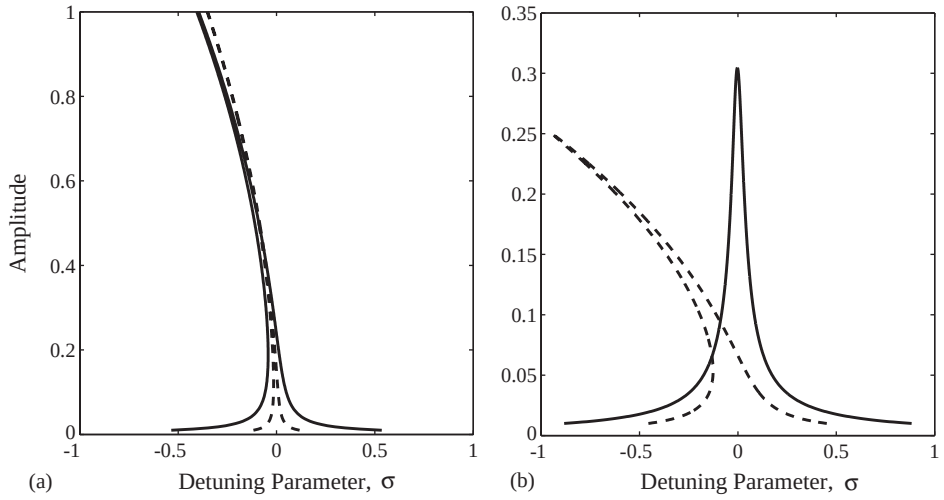

Fig. 5. Non-linear frequency shift of the (a) first and (b) fourth modes for two values of linear stiffness β (solid: $\beta = 500$; dashed: $\beta = 2300$) with $c = 0.025$. These plots illustrate the modal sensitivity to the contact as has been examined previously for linear AFM vibrations [16].

Another important effect in the results is shown in Figs. 4 and 5. In this case, fixed values of F and c are used with results for two different values of linear stiffness β shown. In Fig. 4, amplitude–frequency plots are shown for the first and seconds modes for $\beta = 50$ and 500 ($F = 1$; $c = 0.025$). The frequency shift for the first mode is larger than the second for $\beta = 50$. However, for $\beta = 500$, the second frequency is observed to shift more than the first. In Fig. 5, a comparison between the first and fourth modes is shown for $\beta = 500$ and 2300 ($F = 1$; $c = 0.025$). The fourth

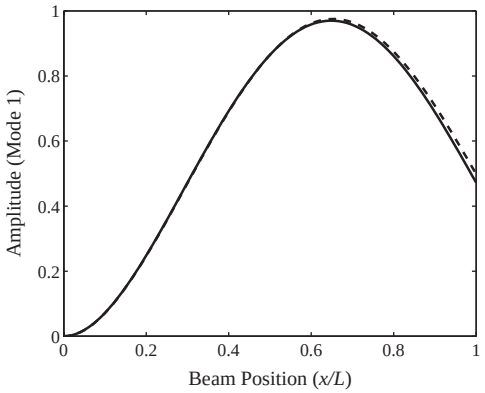

Fig. 6. Comparison between the first linear and the non-linear normal mode (harmonic component) for $\beta = 100$ (—, linear; - - -, non-linear). Note the softening effect of the non-linearity.

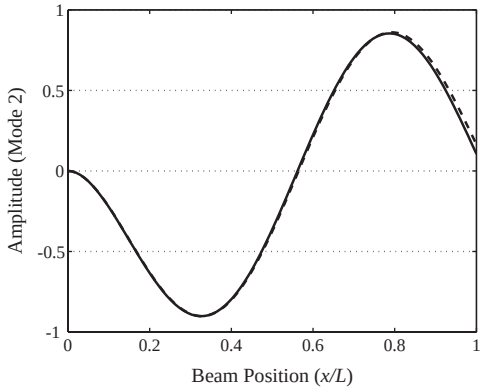

Fig. 7. Comparison between the second linear and the non-linear normal mode (harmonic component) for $\beta = 1900$ (—, linear; - - -, non-linear).

mode is observed to shift much more when $\beta = 2300$ in comparison with the first mode. The behavior of the first mode is very similar for both of these values of β. It was observed that the modal amplitudes and ranges of σ for each mode could be significantly different depending on β. The linear stiffness is primarily dependent on the static surface offset, defined in Eq. (5) by z_0. This type of modal sensitivity has also been noted for the case of an elastic beam coupled to a moving surface by a linear spring [16]. Because the non-linearity is localized to a single position of the beam, the mode shape greatly affects the influence of the non-linearity.

Plots of the harmonic component of the mode shapes are shown in Figs. 6 and 7. In both of these figures, the linear (Eq. (27)) and non-linear (the term in Eq. (58) that multiplies $\cos(\omega t)$) components are shown as solid and dashed lines, respectively. In Fig. 6, the amplitude of the first mode is shown for $\beta = 100$. The linear and non-linear components are almost identical for the portion of the beam closest to the cantilevered end. The difference between the linear and non-linear in this case is at the end ($x = 1$) of the beam. The softening effect is clearly shown. For

large amplitudes, such that the cubic dependency on amplitude is important, the spring is effectively less stiff. Thus, the beam at $x = 1$ has a larger amplitude relative to the linear amplitude. The second mode is shown in Fig. 7 for $\beta = 1900$. A similar behavior is observed for this mode as well. The deviation from linearity is largest at the end with the contact. The deviation of the non-linear mode shapes from the linear mode shapes follows the trend observed for the detuning parameter. For a given value of β, a mode may have a small or large non-linear response. The modal sensitivity to a contact non-linearity is dependent on the linear mode shape.

Finally, plots relevant to the second and third harmonic components of the non-linear responses are shown in Figs. 8–10. In Fig. 8, $G(\chi_2, x)$ for the first mode is plotted for values of linear stiffness $\beta = 10$, 100, 500, and 1000. Although only a few results may be presented here, the general trends observed are summarized. As β increases, the overall amplitude of G decreases and the position of the node moves toward the cantilevered end of the beam. The trends for $G(\chi_2, x)$ for the second and third modes, as shown in Figs. 9 and 10, respectively, are similar to the plot for the first mode in that the amplitude decreases for increasing β. The positions of the nodes of G for these modes are also observed to move toward the cantilevered end of the beam as β increases. In

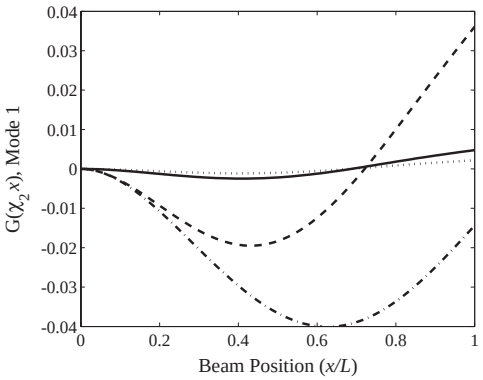

Fig. 8. Plot of $G(\chi_2, x)$ for mode 1 as a function of beam length [$\beta = 10$ (- · -); $\beta = 100$ (- - -); $\beta = 500$ (—); $\beta = 1000$ (. . . .)]. The second harmonic component of the displacement is proportional to G.

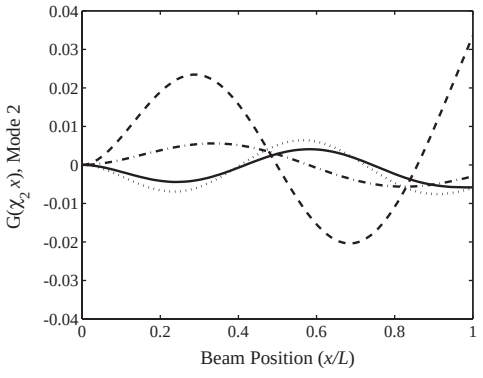

Fig. 9. Plot of $G(\chi_2, x)$ for mode 2 as a function of beam length (key as in Fig. 8). The second harmonic component of the displacement is proportional to G.

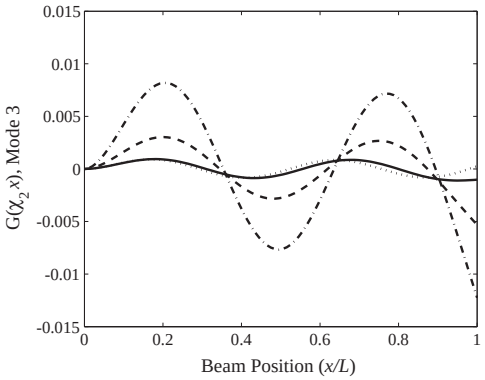

Fig. 10. Plot of $G(\chi_2, x)$ for mode 3 as a function of beam length (key as in Fig. 8). The second harmonic component of the displacement is proportional to G.

addition, it may be observed that an additional node is introduced in these shapes when β is above a certain value. For example, the first mode results, Fig. 8, have a node between $x/L = 0.6-0.7$ for the higher three values of β, but not for $\beta = 10$. For the third mode, Fig. 10, the additional node is only apparent for the highest value of β shown. Thus, each mode has some threshold value of β for which the function G has an increase in number of nodes.

5. Discussion

The non-linear vibrations of a beam with cantilever-Hertzian contact boundary conditions have been investigated using the method of multiple scales. The non-linear amplitude–frequency relation was derived and was shown to depend on the mode number and linear contact stiffness. The linear contact stiffness is primarily dependent on the static offset of the surface. Example results show the expected softening behavior in terms of the forcing amplitude and damping. These results may also be used to predict which modes may be most suitable for non-linear experiments. In particular, it was observed that the first mode lost contact ($p > 1$) in many cases before a significant change in frequency was achieved. The derivation of the non-linear normal modes was also presented. The non-linear modes included terms of a modification to the harmonic linear mode, a static offset, and second and third harmonic components.

The non-linear analysis showed the amplitude–frequency shift that has been observed experimentally in the weakly non-linear regime for atomic force microscope experiments [8]. These non-linear effects provide important information about the contact mechanics. The non-linear behavior of the beam vibrations have been analyzed here using a Hertzian contact model for the tip–surface interaction. The results showed that the influence of the non-linearity on each mode is a function of the surface stiffness relative to the stiffness of the cantilever. The modal sensitivity is also seen to influence the non-linear behavior. Each mode has a different amplitude near the end of the beam such that the role of the non-linearity changes. Results from other contact models will provide necessary insight into the expected effects from other factors important for AFM imaging.

Acknowledgements

This work was sponsored by the Air Force Office of Scientific Research under Grant No. F49620-99-1-0254. The views and conclusions contained herein are those of the authors and should not be interpreted as necessarily representing the official policies or endorsements, either expressed or implied, of the Air Force Office of Scientific Research or the US Government. Support of the Center for Electro-Optics at the University of Nebraska-Lincoln is also gratefully acknowledged.

References

[1] P.R. Nayak, Contact vibrations, *Journal of Sound and Vibration* 22 (1972) 297–322.
[2] M.D. Bryant, Nonlinear forced oscillation of a beam coupled to an actuator via Hertzian contact, *Journal of Sound and Vibration* 99 (1985) 403–414.
[3] D.P. Hess, A. Soom, Normal vibrations and friction under harmonic loads: Part I—Hertzian contacts, *American Society of Mechanical Engineers, Journal of Tribology* 113 (1991) 80–86.
[4] W. Szemplinska-Stupnicka, *The Behavior of Nonlinear Vibrating Systems*, Kluwer, Dordrecht, 1990.
[5] S.W. Shaw, C. Pierre, Normal modes of vibration for nonlinear continuous systems, *Journal of Sound and Vibration* 169 (1994) 319–347.
[6] A.H. Nayfeh, *Nonlinear Interactions*, Wiley, New York, 2000.
[7] A.F. Vakakis, *Normal Modes and Localization in Nonlinear Systems*, Wiley, New York, 1996.
[8] U. Rabe, E. Kester, W. Arnold, Probing linear and nonlinear tip–sample interaction forces by atomic force acoustic microscopy, *Surface and Interface Analysis* 27 (1999) 386–391.
[9] U. Rabe, S. Amelio, E. Kester, V. Scherer, S. Hirsekorn, W. Arnold, Quantitative determination of contact stiffness using atomic force acoustic microscopy, *Ultrasonics* 38 (2000) 430–437.
[10] N.A. Burnham, A.J. Kulik, G. Gremaud, G.A.D. Briggs, Nanosubharmonics: the dynamics of small nonlinear contacts, *Physical Review Letters* 74 (1995) 5092–5095.
[11] M. Muraoka, W. Arnold, A method of evaluating local elasticity and adhesion energy from the nonlinear response of AFM cantilever vibrations, *JSME International Journal Series A, Solid Mechanics and Material Engineering* 44 (2001) 396–405.
[12] K. Wolf, O. Gottlieb, Nonlinear dynamics of a nonconducting atomic force microscope cantilever actuated by a piezoelectric layer, *Journal of Applied Physics* 91 (2002) 4701–4709.
[13] K.L. Johnson, *Contact Mechanics*, Cambridge University Press, Cambridge, 1985.
[14] D. Maugis, *Contact, Adhesion and Rupture of Elastic Solids*, Springer, Berlin, 2000.
[15] A.H. Nayfeh, D.T. Mook, *Nonlinear Oscillations*, Wiley, New York, 1979.
[16] J.A. Turner, J.S. Wiehn, Sensitivity of flexural and torsional modes of atomic force microscope cantilevers to surface stiffness variations, *Nanotechnology* 12 (2001) 322–330.